JOC The Journal of Organic Chemistry

Featured Article

pubs.acs.org/joc

Mechanistic Aspects of Phosphate Diester Cleavage Assisted by Imidazole. A Template Reaction for Obtaining Aryl Phosphoimidazoles

Mozart S. Pereira,[†] Bárbara Murta,[†] Thaís C. F. Oliveira,[†] Alex M. Manfredi,[‡] Faruk Nome,[‡] Alvan C. Hengge,[§] and Tiago A. S. Brandão*[,†]

[†]Department of Chemistry, ICEX, Federal University of Minas Gerais, Belo Horizonte, MG 31270-901, Brazil

[‡]Department of Chemistry, Federal University of Santa Catarina, Florianópolis, SC 88040-900, Brazil

[§]Department of Chemistry and Biochemistry, Utah State University, Logan, Utah 84322-0300, United States

Supporting Information

ABSTRACT: Phosphoimidazole-containing compounds are versatile players in biological and chemical processes. We explore catalytic and mechanistic criteria for the efficient formation of cyclic aryl phosphoimidazoles in aqueous solution, viewed as a template reaction for the in situ synthesis of related compounds. To provide a detailed analysis for this reaction a series of *o*-(2′-imidazolyl)naphthyl (4-nitrophenyl) phosphate isomers were examined to provide a basis for analysis of both mechanism and the influence of structural factors affecting the nucleophilic attack of the imidazolyl group on the phosphorus center of the substrate. Formation of the cyclic aryl phosphoimidazoles was probed by NMR and ESI-MS techniques. Kinetic experiments show that cyclization is faster under alkaline conditions, with an effective molarity up to 2900 M for the imidazolyl group, ruling out competition from external nucleophiles. Heavy atom isotope effect and computational studies show that the reaction occurs through a $S_N2(P)$-type mechanism involving a pentacoordinated phosphorus TS, with apical positions occupied by the incoming imidazolyl nucleophile and the *p*-nitrophenolate leaving group. The P−O bond to the leaving group is about 50−60% broken in the transition state.

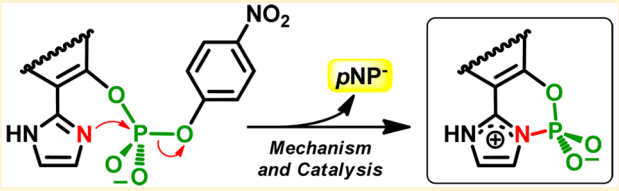

INTRODUCTION

Phosphoimidazole-containing compounds are key intermediates in many biological processes and particularly versatile phosphorylating reagents. Examples of their application are the use of a phosphorimidazolide nucleotide for nonenzymatic template-directed primer extension[1] and the replacement of a 5′-triphosphate nucleotide by 5′-phosphorimidazolide as an efficient electrophilic reaction partner for the DNA-catalyzed modification of a lysine residue in a DNA-anchored peptide substrate.[2]

In biological systems, the interplay between histidine phosphorylation and phosphohistidine dephosphorylation is key for control of the biological activity[3−5] and a striking feature in the mechanism of catalysis of some phosphatases.[6−8] Histidine phosphorylation is implicated in the action of histones and, therefore, in many processes involving DNA replication and transcription.[9,10] Phosphohistidine is estimated to make up 5−7% of nuclear proteins, comparable with the amount of phosphothreonine though lower than phosphoserine and much higher than phosphotyrosine (ca. 1%).[11,12]

Catalysis of P−O bond cleavage by a number of enzymes follows a two-step ping−pong mechanism in which the first catalytic step is nucleophilic attack of a histidine imidazolyl group on the phosphorus atom of the substrate.[13−19] This yields a phosphohistidine intermediate that is converted to products in the second step by reaction with an external nucleophile. Members of the phospholipase D (PLD) family, including Mg^{2+}-independent type-II restriction endonucleases, catalyze the cleavage of phosphate diesters by this mechanism.[8,13,20,21] These enzymes are among the few examples capable of catalyzing the hydrolysis of phosphate diesters without aid of metal ions. Enzymatic rates around 0.3 s^{-1} are over 10^{13}-fold greater than uncatalyzed hydrolysis rates of alkyl phosphate diesters, which are estimated at 10^{-14} s^{-1} under neutral conditions at 25 °C.[22,23] A second histidine residue is involved in each catalytic step of the proposed mechanism of the PLD reaction. The protonated form of an imidazolyl group acts in the first step as a general acid to assist leaving group departure, and then in the second step its neutral form catalyzes water attack by general base catalysis (Figure 1).[13,24]

The structural and electronic factors responsible for PLD proficiency have been subject of intense debate.[25,26] The combination of nucleophilic and general acid catalysis as in **1** (Scheme 1), a model for the first step of the PLD reaction, was proposed to account for its 10^{11}-fold faster hydrolysis compared to diphenyl phosphate. Reaction occurs in two steps, and detectable levels of the *N*-methylphosphoimidazole **2** were observed by FTICR-MS, suggesting its formation to be at least of the same order of magnitude or faster than its cleavage.[26]

Received: June 5, 2016
Published: July 8, 2016

DOI: 10.1021/acs.joc.6b01358
J. Org. Chem. 2016, 81, 8663−8672

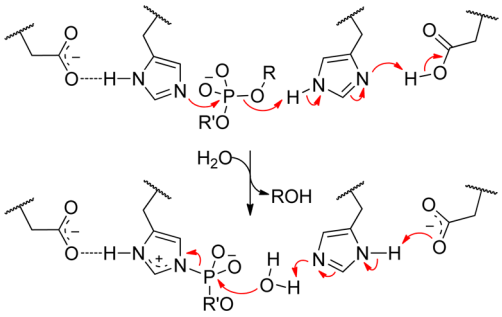

Figure 1. Proposed mechanism for phospholipase D family members.

We report the cleavage of constitutional isomers of the *o*-(2′-imidazolyl)naphthyl (4-nitrophenyl) phosphate (NIP-*p*NP)[27] termed 1NI2P-*p*NP, 2NI1P-*p*NP, and 3NI2P-*p*NP based on the naphthalene ring positions of the imidazolyl and phosphoryl groups (Scheme 2). The side-by-side positions of the imidazolyl and phosphoryl groups on the naphthalene ring provide the basis for the analysis of subtle variations in the geometric requirements for efficient intramolecular nucleophilic catalysis. The cleavage of these compounds provides a PLD model for the first catalytic step with a "simple" imidazolyl nucleophile displacing a leaving group with known acidity. The NIP-*p*NP cleavage affords cyclic aryl phosphoimidazoles. We show that these compounds are stable under reaction conditions that provide an efficient NIP-*p*NP cleavage, so we can explicitly probe the efficiency of the nucleophilic catalysis in the first catalytic step. The amount of kinetic data for the formation of aryl phosphoimidazoles is limited and this study provides useful chemical information for the design of phosphorylating agents. The naphthalene derivatives provide two distinct *ortho* substitutions (1,2 and 2,3) with structural and reactivity consequences for NIP-*p*NP cleavage, which offer an efficient template reaction for obtaining aryl phosphoimidazoles.

RESULTS AND DISCUSSION

Identification of Reagents and Products. Figures S1−S3 show the ^{1}H, ^{31}P, and ^{13}C NMR spectra in DMSO-d_6 for the *o*-(2′-imidazolyl)naphthyl (4-nitrophenyl) phosphate (NIP-*p*NP) obtained by our synthetic procedures (see the Experimental Section). Reaction products for the NIP-*p*NP cleavage in water were identified by ^{1}H and ^{31}P NMR and ESI-MS(/MS). The NIP-*p*NP cleavage yielded the corresponding cyclic aryl phosphoimidazoles termed here as NIP*c*. Figure 2 presents the NMR spectra for the reaction of 1NI2P-*p*NP in 0.01 M NaOD at 21 °C, and the corresponding data for 2NI1P-*p*NP and 3NI2P-*p*NP are depicted in Figures S4 and S5. The NMR signals observed in these reactions, and their assignments are shown in Table 1. Scheme 3 considers these observations and the kinetic studies discussed further in this work.

Scheme 2. Structure of the *o*-(2′-Imidazolyl)naphthyl (4-Nitrophenyl) Phosphate Diesters Studied in This Work

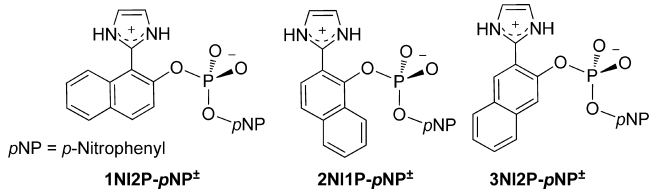

The ^{31}P NMR signals in the course of the NIP-pNP cleavage do not differ significantly. The 1NI2P-*p*NP signal at −10.3 ppm disappeared under basic conditions to give a stable product (1NI2P*c*$^{-}$) at −12.9 ppm (Figure 2a), and the corresponding ^{31}P NMR signals for the 2NI1P-*p*NP and 3NI2P-*p*NP are found to be close to these values. The reaction solutions turn increasingly yellow over time due to *p*-nitrophenolate (*p*NP^{-}) formation. Relative concentrations of species obtained by ^{31}P NMR in the course of each reaction are presented in Figure 3, and the data follow typical first-order kinetic behavior.

Figures 2b shows the ^{1}H NMR spectra at the beginning and end (at least 90% complete) of the 1NI2P-*p*NP reaction. Peaks of 1NI2P-*p*NP at 7.08 and 8.16 ppm (at 2.5 min) disappeared to give signals with the same coupling constant (J = 9.1 Hz) at 6.61 and 8.08 ppm (at 180 min) and identified as *p*-nitrophenolate from direct comparison to a standard sample. Most chemical shifts for hydrogen atoms at the naphthalene ring overlap between 7.3 and 8.1 ppm precluding signal attribution. Nevertheless, the appearance of a signal at 9.39 ppm (1H, duplet, J = 8.5 Hz) is likely to belong to the H-8 at the α position of the naphthalene moiety of 1NI2P*c*$^{-}$. Hydrogen atoms at position 8 are known to interact with neighboring groups at position 1 by the so-called "*peri* effect",[28−30] which in our case involves the deprotonated nitrogen atom of the phosphoimidazolyl group.

The ^{1}H NMR spectra for 2NI1P-*p*NP and 3NI2P-*p*NP, presented in Figures S4 and S5, differ mainly in the naphthalene hydrogen signal positions. Worth mentioning is the appearance of a signal at 9.47 ppm (1H, duplet, J = 8.7 Hz) for the reaction of 2NI1P-*p*NP, assigned to the H-8 deshielded by the oxygen atom bound at the *peri* position of the naphthalene moiety of 2NI1P*c*$^{-}$. However, in the absence of any group at the α position of the naphthalene ring as observed for 3NI2P*c*$^{-}$, the *peri* effect is not observed and the most deshielded signal at the end of the 3NI2P-*p*NP cleavage is observed upfield at 8.50 ppm (1H, singlet). The NIP-*p*NP cleavage shows no spectral evidence for the formation of *o*-(1*H*-imidazol-2-yl)naphthols as provided by direct comparison with pure samples of these compounds.

The reacting species for the NIP-*p*NP cleavage were transferred directly from solution into the gas phase and detected by ESI-MS in the negative ion mode. Figure 4 shows

Scheme 1. PLD Enzyme Mimic Combining Nucleophilic and General Acid Catalysis

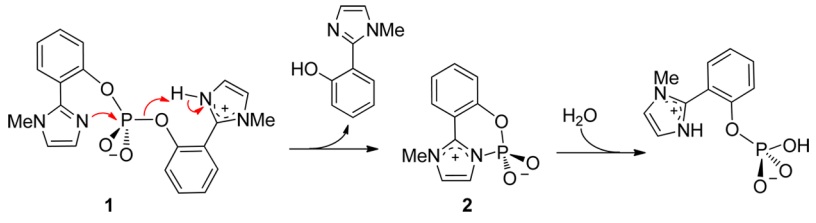

DOI: 10.1021/acs.joc.6b01358
J. Org. Chem. 2016, 81, 8663−8672

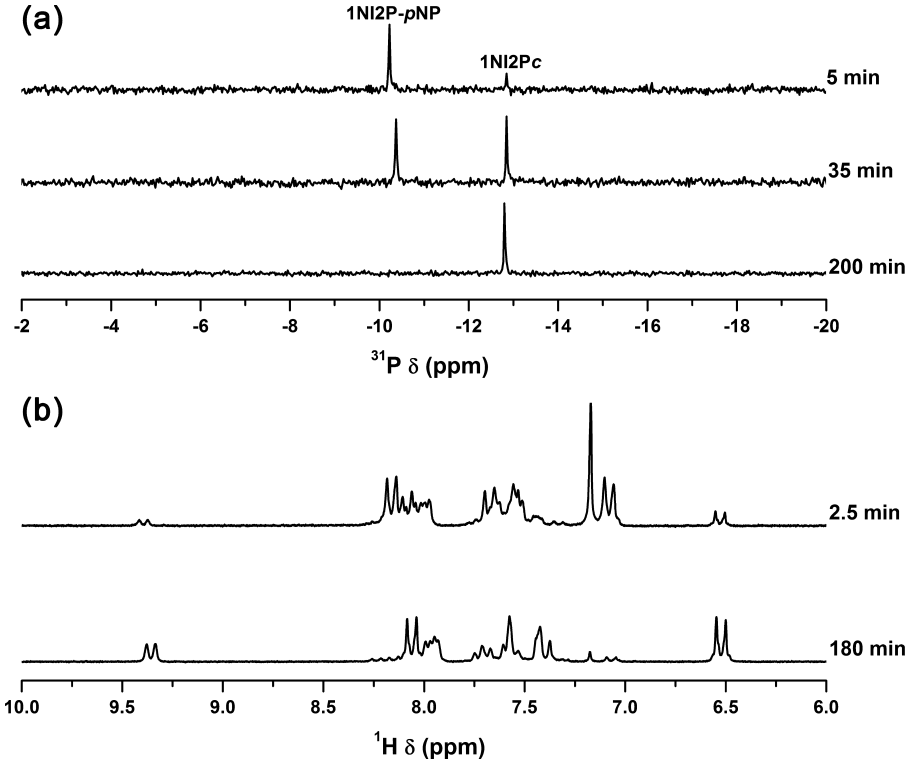

Figure 2. (a) ^{31}P NMR (81 MHz) and (b) ^{1}H NMR (200 MHz) spectra at different time intervals for the cleavage of 1NI2P-*p*NP in 0.01 M NaOD at 21 °C.

Table 1. Signals and Assignments for Reagents and Products in the NIP-*p*NP Cleavage in 0.01 M NaOD at 21 °C

compd	^{1}H NMR δ (ppm)	^{31}P NMR δ (ppm)
1NI2P-*p*NP$^-$	7.08 (2H, d, J = 9.1 Hz), 7.17 (2H, s), 7.49−7.60 (2H, m), 7.61−7.73 (2H, m), 7.95−8.13 (2H, m), 8.16 (2H, d, J = 9.1 Hz)	−10.3
1NI2P*c*$^-$	7.36−7.50 (2H, m), 7.52−7.67 (2H, m), 7.73 (1H, t, J = 7.7 Hz), 7.92−8.05 (2H, m), 9.39 (1H, d, J = 8.5 Hz)	−12.9
2NI1P-*p*NP$^-$	7.11−7.35 (4H, m), 7.55−7.71 (2H, m), 7.74−7.94 (2H, m), 8.00−8.20 (2H, m), 8.26 (2H, d, J = 7.9 Hz)	−10.9
2NI1P*c*$^-$	7.42−7.56 (2H, m), 7.57−7.71 (2H, m), 7.78 (1H, t, J = 7.5 Hz), 7.98−8.15 (2H, m), 9.47 (1H, d, J = 8.7 Hz)	−14.3
3NI2P-*p*NP$^-$	7.07 (2H, d, J = 9.0 Hz), 7.17 (2H, s), 7.47−7.66 (2H, m), 7.89 (1H, d, J = 7.7 Hz), 7.93−8.01 (2H, m), 8.05 (2H, d, J = 9.0 Hz), 8.30 (1H, s)	−10.5
3NI2P*c*$^-$	7.34 (1H, br s), 7.47−7.66 (3H, m), 7.75 (1H, s), 7.90 (1H, d, J = 7.6 Hz), 8.04 (1H, d, J = 8.7 Hz), 8.50 (1H, s)	−12.6
*p*NP$^-$	6.59 ± 0.09 (2H, d, J = 9.2 ± 0.3 Hz), 8.08 ± 0.02 (2H, d, J = 9.2 ± 0.3 Hz)[a]	

[a]Average for NMR observations at the end of 1NI2P-*p*NP, 2NI1P-*p*NP, and 3NI2P-*p*NP cleavages.

Scheme 3. Reaction Pathway for NIP-*p*NP Cleavage

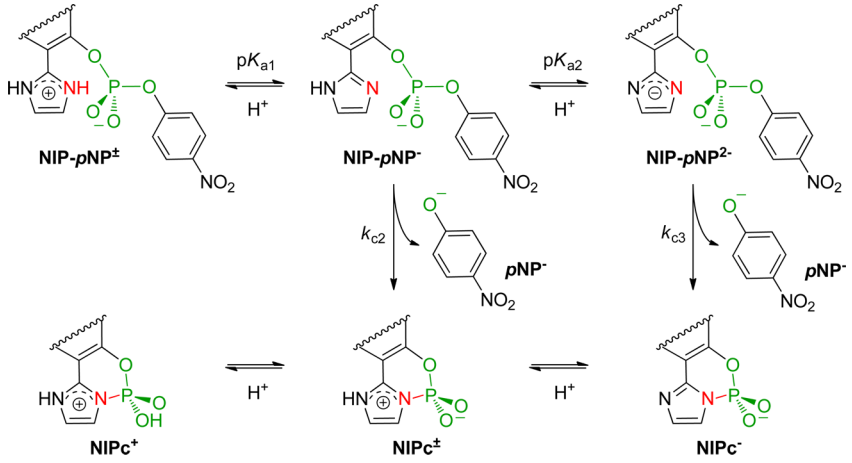

the ESI-MS data for the 1NI2P-*p*NP reaction in NaOH 5 mM. The 1NI2P-*p*NP$^-$ observed at the beginning of the reaction at m/z 410.05 disappears over time, and major species after 40 min of reaction are 1NI2P*c*$^-$ and *p*NP$^-$ at m/z 271.03 and

DOI: 10.1021/acs.joc.6b01358
J. Org. Chem. 2016, 81, 8663−8672

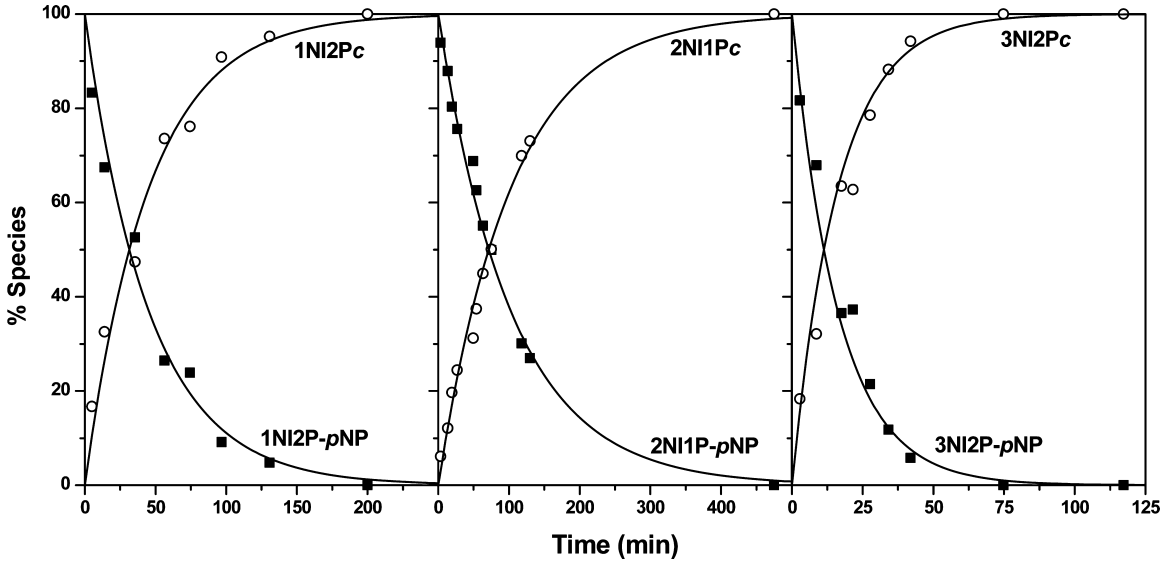

Figure 3. Relative concentrations of species obtained by ^{31}P NMR over the course of NIP-*p*NP cleavage in 0.01 M NaOD at 21 °C. Solid lines are first-order kinetic fits with rate constants of 3.7 × 10^{-4} s^{-1}, 1.7 × 10^{-4} s^{-1}, and 1.0 × 10^{-3} s^{-1} for 1NI2P-*p*NP, 2NI1P-*p*NP, and 3NI2P-*p*NP reactions, respectively.

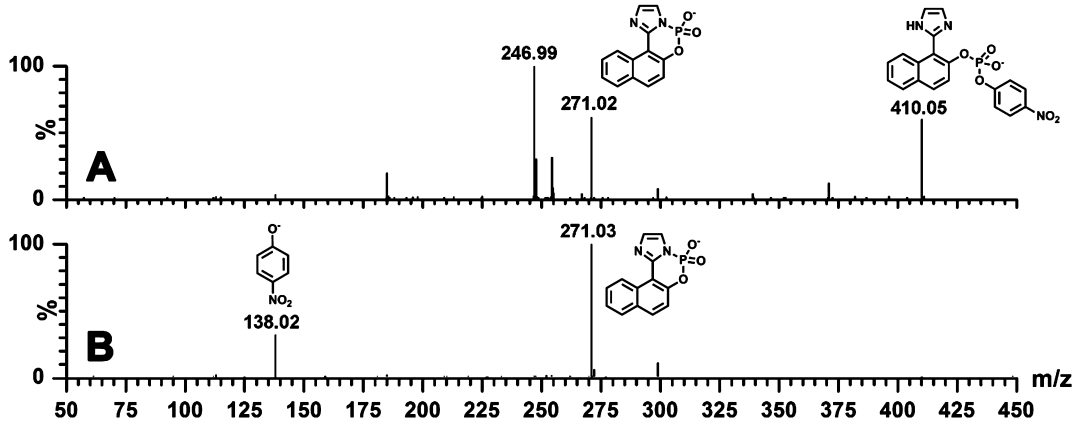

Figure 4. ESI-MS (negative ion-mode) for the cleavage of 1NI2P-*p*NP in 5 mM NaOH at the beginning (spectra A) and end of the reaction (spectra B) at 19 °C.

138.02, respectively. These data essentially mirror the ESI-MS data in Figures S6 and S7 for the respective 2NI1P-*p*NP and 3NI2P-*p*NP cleavages in pH 8.5 (NH_4OH 5.0 mM). Species formed over the course of the reactions were identified by ESI-MS/MS via their unimolecular dissociation chemistry (Figures S8−S10).

Effect of pH on the Kinetic Rates. Figure 5 shows pH−rate profiles for NIP-*p*NP cleavage at 45 °C. The reaction rates depend on the molar fractions of the NIP-*p*NP ionic species shown in Scheme 3 and are described by the logarithmic form of eq 1. The individual rate constants and pK_a values determined from fits of the data appear in Table 2.

$$k_{obs} = \frac{k_{c2}}{\left(\frac{[H^+]}{K_{a1}} + 1 + \frac{K_{a2}}{[H^+]}\right)} + \frac{k_{c3}}{\left(\frac{[H^+]^2}{K_{a1}K_{a2}} + \frac{[H^+]}{K_{a2}} + 1\right)} \quad (1)$$

The NIP-*p*NP cleavage is faster under alkaline conditions and proceeds with stoichiometric formation of *p*-nitrophenolate, as determined by UV−vis spectroscopy, taking into consideration its molar absorptivity of 18320 M^{-1} cm^{-1} at 400 nm in water.[31] The constants k_{c2} and k_{c3} denote the respective spontaneous cleavage of the mono- and dianionic species of NIP-*p*NP, and pK_{a1} and pK_{a2} refer to the acidity constants for deprotonation of the corresponding conjugated acids that yield these species (Scheme 3). These values are consistent with the pK_a values determined for imidazole[32−34] and derivatives.[26,29,35] The NIP-*p*NP cleavage is 2.5- to 12-fold faster than the hydrolysis of BMIPP **1** (k = 5.43 × 10^{-4} s^{-1} at 45.0 °C).[26] The cleavage of the zwitterionic species of NIP-*p*NP by k_{c1} was too slow to be measured and so was neglected in the fitting.

Effective Molarity of the Imidazolyl Group. The formation of the cyclic aryl phosphoimidazoles NIP*c* as probed by NMR and ESI-MS(/MS), and the results from pH−rate profiles, demonstrate that NIP-*p*NP cleavage occurs solely by intramolecular nucleophilic attack of the imidazolyl group or its conjugate base. This reaction is fast compared to the cleavage of other phosphate esters. The rate for the spontaneous hydrolysis of bis(*p*-nitrophenyl) phosphate is estimated as 1.71 × 10^{-10} s^{-1} from the $\Delta H^{\ddagger}$ = 24.8 kcal/mol and $\Delta S^{\ddagger}$ = −25.4 eu,[36] which is about 2 × 10^7-fold lower than the rate for cleavage of the NIP-*p*NP anionic species (k_{c2} in Table 2) at the same temperature. We note that a more suitable catalytic rate may be

DOI: 10.1021/acs.joc.6b01358
J. Org. Chem. 2016, 81, 8663−8672

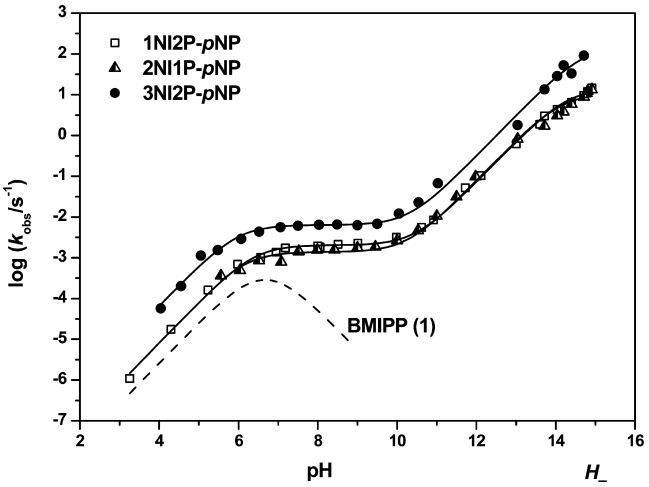

Figure 5. pH−rate profiles for the NIP-*p*NP cleavage reactions at 45.0 °C and ionic strength of 1.0 (KCl). The solid curves are fits according to eq 1 using the equilibrium and rate constants shown in Table 2. The pH scale refers to the region between 2 and 14; above pH 14, the H_ basicity function was used. For comparison purposes, the pH−rate profile for the hydrolysis of BMIPP **1** at 45.0 °C is shown as a dashed line; estimated from data in Table 3 in the report by Orth et al.[26]

Table 2. Kinetic Parameters for the NIP-*p*NP Cleavage at 45.0 °C and Ionic Strength of 1.0 (KCl)

constant	1NI2P-*p*NP	2NI1P-*p*NP	3NI2P-*p*NP
k_{c2}, 10^{-3} s^{-1}	2.03 ± 0.09	1.39 ± 0.08	6.35 ± 0.05
k_{c3}, s^{-1}	14.3 ± 0.6	10.7 ± 0.9	154 ± 15
pK_{a1}	6.40 ± 0.04	6.17 ± 0.08	5.98 ± 0.06
pK_{a2}	14.30 ± 0.03	14.14 ± 0.05	14.69 ± 0.05

calculated from the spontaneous hydrolysis of *p*-nitrophenyl phenyl phosphate, but the non-leaving group effect for exchanging phenyl to *p*-nitrophenyl is small. We base this assumption on an observed β_{NLG} of only −0.031 for the dependence of the hydrolysis rates of aryl 2,4-dinitrophenyl phosphates with the pK_a of the nonleaving group,[37,38] which is too small to affect our prediction significantly.

Effective molarities (EM) of about 450, 410, and 2900 M, respectively, for 1NI2P-*p*NP$^-$, 2NI1P-*p*NP$^-$, and 3NI2P-*p*NP$^-$ are obtained from the ratio of the rate constants for the intramolecular nucleophilic attack of the imidazolyl group on the phosphorus atom (k_{intra} = k_{c2} values at 25 °C) and the second-order rate constant (k_{inter} = 7 × 10^{-7} M^{-1} s^{-1} at 25 °C) for the intermolecular attack of imidazole (pK_{nuc} = 7.1) on a phosphate diester of pK_{lg} = 7.15 (*p*-nitrophenol). The k_{c2} values at 25 °C are found in the Supporting Information. The k_{inter} was predicted from the second-order rate constant for the nucleophilic attack of imidazole on bis(2,4-dinitrophenyl) phosphate (k = 1.42 × 10^{-3} M^{-1} s^{-1} at 25 °C, pK_{lg} = 4.07)[39] and a β_{lg} = −1.07 at 25 °C (−1.02 at 39 °C) for the reaction of methyl aryl phosphates with a nitrogen nucleophile with pK_{nuc} of 7.1.[40] Details of this estimation are provided in the Supporting Information.

The EM values for the NIP-*p*NP$^-$ are large, although lower than observed for the nucleophilic catalysis for compounds **3** and **4**, for which the amine-[41] and pyridine-like[42] intramolecular nucleophiles have EM of about 1.6 × 10^5 M^{-1} and 7000 M^{-1}, respectively. The formation of cyclic intermediates in phosphate ester hydrolysis seems to be a favored mechanism for compounds involving O- or N-nucleophiles and five- or six-membered cyclic transition states. Nucleophilic attack seems not to be favored for four-membered ring transition states, as observed for compound **5**, for which kinetic and computational evidence indicates that the pyridinyl moiety acts as a general-base catalyst for the nucleophilic attack of a water molecule.[43] In all cases, the departure of the leaving group occurs in line with the nucleophilic attack. We rationalize the lower EM values for the imidazolyl group of the NIP-*p*NP$^-$ relative to the secondary amine in **3** and the quinolinic nitrogen atom in **4** result from the respective lower basicity of the imidazolyl moiety and orbital steering effects[44,45] that reduce the number of conformers in productive geometries for catalysis.[46]

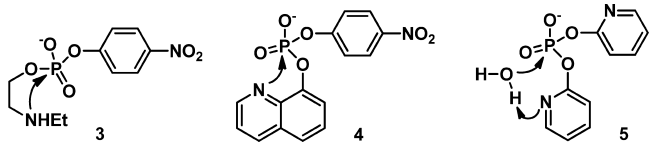

Effect of General Bases and Solvent Isotope Effect. The estimated EM values for the nucleophilic attack of the imidazole group in the NIP-*p*NP are considerable. We observe that rate constants for 1NI2P-*p*NP$^-$ cleavage are not increased by adding external nucleophiles as acetate, hydrogen phosphate, or even hydroxylamine (Table 3), a powerful nucleophile able to accelerate the cleavage of phosphate diesters by about 10^6- and 10^3-fold compared to water or a nucleophile with the same pK_a.[47]

Table 3. Effect of Added General Bases and Nucleophiles on the Cleavage of 1NI2P-*p*NP[a]

general bases/conditions	k_{obs}, 10^{-4} s^{-1}
H_2O, pH 8.0 (Tris 0.01 M), 25.0 °C	3.23
acetate 0.6 M, pH 8.0 (Tris 0.01 M), 25.0 °C	3.19
acetate 1.0 M, pH 8.0 (Tris 0.01 M), 25.0 °C	3.26
H_2O, pH 8.0 (Tris 0.01 M), 45.0 °C	19.2
NH_2OH 1.0 M, pH 8.0 (Tris 0.01 M), 45.0 °C	19.9
H_2O, pH 9.0 (Tris 0.01 M), 45.0 °C	22.5
phosphate 0.4 M, pH 9.0 (Tris 0.01 M), 45.0 °C	21.3

[a]Ionic strength = 1.0 (KCl) for all reactions.

The independence of catalytic rates on general base concentration shows that general-base catalysis is too slow to be observed. General-base catalysis could occur by a concerted deprotonation of the distal N−H imidazolyl group by the general base with an increase of the electronic density at the nucleophilic N atom during attack. This form of activation has been proposed for PLD[13,48,49] and other hydrolases[50,51] with aspartate (as general base) and histidine (as nucleophile) residues in the active site. However, a LBHB without full proton transfer between these residues is more likely.[52] The catalytic effects of an intramolecular acetate group are modest in other reported enzyme models; Komiyama[53] observed that 4-imidazole acetate accelerated the cleavage of bis(2,4-dinitrophenyl) phosphate (BDNPP) by only 4.6-fold compared to an unsubstituted imidazole, and the kinetic solvent isotope effect (KSIE) for k_{cat}(in H_2O)/k_{cat}(in D_2O) = 2.3 was in agreement with the role of the acetate group as an intramolecular general-base catalyst.

Rate constants for the NIP-*p*NP cleavage in H_2O and D_2O were measured at pH 8.50 (Table 4) showing KSIE values lower than 1.3, a low value not consistent with general-base

DOI: 10.1021/acs.joc.6b01358
J. Org. Chem. 2016, 81, 8663−8672

Table 4. Kinetic Solvent Isotope Effect (k_{H_2O}/k_{D_2O}) for the NIP-*p*NP Cleavage in pH(D) 8.50 at 45.0 °C and Ionic Strength of 1.0 (KCl)[a]

compd	k_{H_2O}, 10^{-3} s^{-1}	k_{D_2O}, 10^{-3} s^{-1}	k_{H_2O}/k_{D_2O}
1NI2P-*p*NP[b]	2.12	1.73	1.23
2NI1P-*p*NP	1.57	1.48	1.06
3NI2P-*p*NP	6.50	5.14	1.27

[a] k_{H_2O} and k_{D_2O} are observed rate constants. [b] k_{H_2O}/k_{D_2O} at pH(D) 8.00 and 9.01 were 1.19 and 1.31, respectively; calculated from k_{H_2O} = 1.92 × 10^{-3} s^{-1} and k_{D_2O} = 1.62 × 10^{-3} s^{-1} at pH(D) 8.00 and k_{H_2O} = 2.26 × 10^{-3} s^{-1} and k_{D_2O} = 1.73 × 10^{-3} s^{-1} at pH(D) 9.01.

catalysis. Nome et al. observed a similar KSIE of 1.2 for the intermolecular reaction of BDNPP with 1 M imidazole at pH 8.5.[39] These observations indicate that in the absence of a well-positioned general base the reactions are nucleophilic in nature. We also observe that the increase in the rate constant at pH >10 for the formation of the cyclic aryl phosphoimidazole involves specific base catalysis: the imidazolate formed from deprotonation of imidazole is evidently a better nucleophile than hydroxide ion. Of course, nucleophilic attack by hydroxide ion would give no cyclic intermediate, different from what we observe in the NMR and ESI-MS data.

Since the NIP-*p*NP cleavage proceeds exclusively with the intramolecular nucleophilic attack of imidazolyl or imidazolate group, the extent of nucleophilic participation of these groups in the transition state may be obtained from analysis of the Brønsted parameter β_{nuc}, determined from the linear correlation of the rate constants k_{c2} and k_{c3} for the respective imidazole and imidazolate with their corresponding conjugated acids' pK_a values (Table 2). A β_{nuc} value of 0.50 is calculated for the three NIP-*p*NP isomers. Although this analysis is tentative due to the absence of more kinetic data, the imidazolyl and imidazolate groups in the NIP-*p*NP have similar spatial arrangements in relation to the phosphorus atom but quite distinct nucleophilicities, affording a proper relationship. The β_{nuc} values for the NIP-*p*NP cleavage are higher than determined for the reaction of methyl 2,4-dinitrophenyl phosphate with oxygen and nitrogen nucleophiles (β_{nuc} = 0.30),[40] and similar to the β_{nuc} of 0.41 determined for the reaction of ethyl 2,4-dinitrophenyl phosphate with α-nucleophiles.[54] In each case, these values are indicative that the reaction proceeds via a $S_N2(P)$-type mechanism in a pentacoordinated transition state. The larger β_{nuc} value observed for the NIP-*p*NP cleavage is consistent with increased bond formation between the nucleophile and phosphorus atom regarding nucleophiles without activation. Such an effect occurs internally for imidazole by electronic distribution from the distal nitrogen atom (non-nucleophilic) to the nucleophilic nitrogen atom.

Heavy Atom Isotope Effect. The extent of P−O bond fission in the transition state of the NIP-*p*NP cleavage was obtained from measurements of the secondary nitrogen-15 kinetic isotope effect (^{15}k KIE) in the leaving group NO_2 group of 1NI2P-*p*NP (Table 5). This KIE is sensitive to negative charge formed from P−O bond cleavage on the leaving group, by delocalization into the nitro group. Background for interpretation of ^{15}k KIE data is provided by a number of determinations in the literature;[55] see Table 5 for reference data. The *p*-nitrophenyl phosphate dianion, a typical phosphate monoester, hydrolyzes through a loose transition state with

Table 5. Nitrogen-15 Kinetic Isotope Effects (^{15}k) for Cleavage of 1NI2P-*p*NP and Different Phosphate Esters for Comparison Purposes[56]

reaction/conditions	^{15}k KIE[a]
1NI2P-*p*NP cleavage, pH 9.0, 22 °C	1.0021(1)
*p*NPP dianion hydrolysis, 95 °C	1.0028(2)
EtO*p*NPP monoanion hydrolysis, 95 °C	1.0010(1)
range of phosphodiester data	1.0007−1.0016

[a] Values in parentheses after KIE are standard errors in the last decimal place.

nearly a full negative charge on the leaving group. Its high ^{15}k values (>1.0028) provides an estimation of the upper bound expected for this isotope effect. In contrast, ^{15}k values for phosphate diesters range between 1.0007 and 1.0016, typical for reactions showing tighter, more synchronous transition states with modest to partial charge formation on the leaving group. The ^{15}k KIE for 1NI2P-*p*NP cleavage is approximately 2/3 of its maximum value[55] of about 1.003, and higher than observed for reactions of most phosphate diesters implying a $S_N2(P)$-type transition state with extensive P−O bond cleavage and large charge development in the leaving group.

Thermodynamic Parameters. Kinetic studies at different temperatures and pH values were carried out for the NIP-*p*NP cleavage (Figures S11, S13, and S15). Analysis of these data according to eq 1 provides the k_{c2} values at different temperatures (Tables S2−S4), which were employed with use of the Eyring plots (Figures S12, S14, and S16) for determination of the activation parameters for NIP-*p*NP^- cleavage (Table 6).

Table 6. Thermodynamic Parameters for Cleavage of the Monoanionic Species of the NIP-*p*NP at an Ionic Strength of 1.0 (KCl)[a]

compd	$\Delta H^{\ddagger}$ (kcal mol^{-1})	$\Delta S^{\ddagger}$ (eu)	$\Delta G^{\ddagger}$[b] (kcal mol^{-1})
1NI2P-*p*NP	16.22 ± 0.02	−20.49 ± 0.05	22.33 ± 0.02
2NI1P-*p*NP	14.89 ± 0.02	−25.22 ± 0.05	22.40 ± 0.02
3NI2P-*p*NP	13.33 ± 0.03	−27.45 ± 0.08	21.51 ± 0.04

[a] Calculated using the Eyring equation and the k_{c2} values determined from data fit of pH−rate profiles at different temperatures; [b] At 25.0 °C.

The significant negative $\Delta S^{\ddagger}$ reflect the need for a specific geometrical alignment for a reactive conformation, despite its unimolecular nature. These values also indicate a greater degree of solvation of the transition state relative to the initial state due to charge dispersal involving the leaving group. The $\Delta S^{\ddagger}$ and $\Delta H^{\ddagger}$ values further decrease in the order 1NI2P-*p*NP, 2NI1P-*p*NP, and 3NI2P-*p*NP, indicating that differential geometric characteristics influence the reactivity of these compounds.

Near-attack conformers (NAC) have been implicated in reactions of constitutional isomers and parent molecules that react over the same reaction coordinate.[57−59] NAC is a reactive state with proper geometric requirements and is in equilibrium with nonreactive NACs. As this equilibrium precedes the formation of the transition state, the NAC population correlates with reactivity. For the NIP-*p*NP, the NAC state requires the imidazolyl and phosphoryl groups to be in close proximity, and the lowest $\Delta H^{\ddagger}$ value for 3NI2P-*p*NP among the series correlates with less geometric restraints for NAC formation.

DOI: 10.1021/acs.joc.6b01358
J. Org. Chem. 2016, 81, 8663−8672

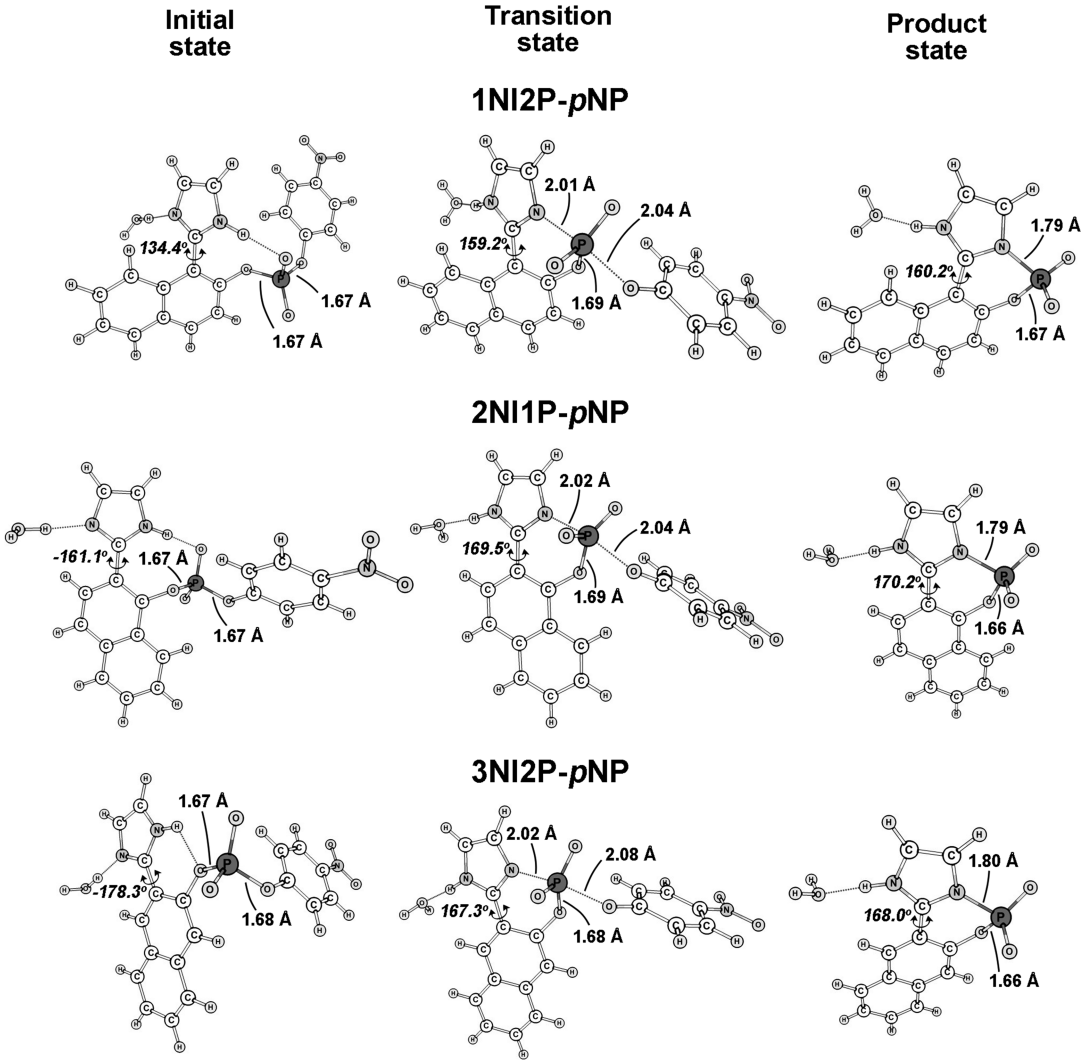

Figure 6. Structures for the initial, transition and product states of the NIP-pNP cleavage optimized at the B3LYP/6-31+G(d,p)/SCRF-PCM level. Cartesian coordinates for these structures are found in the Supporting Information (Tables S6−S9).

However, the number of reactive conformers decreases proportionally for all other isomers in which the phosphoryl and imidazolyl groups are spatially arranged for the most part on opposite sides relative to the naphthalene ring. This effect is more substantial for 1NI2P-*p*NP, wherein rotation of the interannular bond is considerably impaired as previously seen for *o*-(2′-imidazolyl)naphthol constitutional isomers.[29] Similarly, the decrease of the $\Delta S^{\ddagger}$ values in the same order observed for the $\Delta H^{\ddagger}$ values can also be explained by the same geometric factors that indicates the initial state of 3NI2P-*p*NP showing a flatter PES compared with the other isomers.

Computational Studies. Ab initio calculations were performed to analyze the conformational factors involved in the NIP-*p*NP cleavage and to draw a comparison with the mechanism proposed from the experimental results. The calculations were carried out at the B3LYP/6-31+G(d,p)/SCRF-PCM level using water as dielectric continuum. An explicit water molecule was included in the solvation of the imidazolyl group to consider specific hydrogen-bonding effects. Figure 6 shows the optimized structures for the initial, transition, and product states of the NIP-*p*NP cleavage along with selected electronic and structural parameters; the structure for pNP^{-} is presented in the Supporting Information. Energies for each structure appear in Table S5. The theoretical and experimental activation free energy ($\Delta G^{\ddagger}$) variations for the NIP-*p*NP cleavage agree remarkable well (Table 7).

Table 7. Theoretical (B3LYP/6-31+G(d,p)/SCRF-PCM Level (Solvent = Water) and Experimental Free Energy Variations (in kcal mol^{-1} at 25.0 °C) for the NIP-*p*NP Cleavage

compd	ΔG° (theor)	$\Delta G^{\ddagger}$ (theor)	$\Delta G^{\ddagger}$ (exp)
1NI2P-*p*NP	−2.0	23.7	22.3
2NI1P-*p*NP	−5.3	21.5	22.4
3NI2P-*p*NP	−2.7	22.7	21.5

The optimized transition states for the NIP-*p*NP cleavage exhibit a $S_N2(P)$ phosphorane-like structure with the nucleophilic imidazolyl's nitrogen atom and *p*-nitrophenolate at the apical positions of the pentacovalent phosphorus center and the equatorial positions occupied by the two nonbridging oxygen atoms and the naphthol moiety (Figure 6). This behavior is expected for a 6-*exo* (apical) being favored in relation to a 6-*endo* (equatorial) transition state. A similar $S_N2(P)$ phosphorane-like transition state was also proposed

DOI: 10.1021/acs.joc.6b01358
J. Org. Chem. 2016, 81, 8663−8672

from KIE, linear free energy relationship (LFER) measurements, and theoretical calculations for the hydrolysis of phosphoimidazole, which is very closely related to the NIP-*p*NP cleavage.[60]

Consistent with the ^{15}k KIE data, the computational studies indicate extensive P−O bond cleavage at the transition state of 1NI2P-*p*NP$^-$ cleavage. The ChelpG charge population on the oxygen atom of the leaving group shows a variation of 0.33 from the initial (−0.50e) to product (−0.83e) state. The transition state (−0.67e) is more negative by 0.17 from the initial state, indicative of about 52% of full P−O bond cleavage.

Despite the similarities above for the NIP-*p*NP cleavages, one should bear in mind that the lowest energy reaction coordinate is flanked by thermally accessible structures. A quick review of the geometric features of structures in Figure 6 reveals that the attack of the imidazolyl group on the phosphorus atom in 1NI2P-*p*NP must pass a narrower reaction coordinate through limited interannular angles between the imidazole and naphthalene rings. However, the other isomers have a broader reaction window, with 3NI2P-*p*NP being the most favorable reaction for steric reasons.

CONCLUSIONS

The formation of the cyclic aryl phosphoimidazoles is easily achieved in stoichiometric yield under alkaline conditions without competition from external nucleophiles. Cyclization occurs through a $S_N2(P)$-type mechanism with extensive P−O bond cleavage with the leaving group. Reactions are fast and complete within a few minutes as a result of favorable geometries for intramolecular nucleophilic attack. The NIP-*p*NP offers advantages over others because the cyclization is followed by deprotonation to afford a stable cyclic aryl phosphoimidazole species. On the contrary, the corresponding cyclic compounds from **1**, **3**, and **4** cannot be easily handled for further applications. For example, the cyclic compound from **3** is less susceptible to reaction with other nucleophiles, and the cyclic compounds from **1** and **4** are too labile to be used for reactions in situ. Studies about the kinetic features of cyclic aryl phosphoimidazoles are well advanced and show that these compounds react quickly under mild acidic conditions.

EXPERIMENTAL SECTION

Materials. Inorganic salts were of analytical grade and were used without further purification. Liquid reagents were purified by distillation. Syntheses of the *o*-(1*H*-imidazol-2-yl)naphthols were performed according to a previous report.[29]

Preparation of NIP-*p*NP (Scheme 2). A mixture of the corresponding *o*-(1*H*-imidazol-2-yl)naphthol (2.3 mmol, 1 equiv) and triethylamine (2.3 mmol, 1 equiv) was prepared in dry chloroform (30 mL). This mixture was added dropwise to neat *p*-nitrophenyl dichlorophosphate (3.40 mmol, 1.5 equiv) under argon atmosphere with EtOH/N_2 cooling bath and magnetic stirring. The reaction mixture was allowed to react overnight at room temperature. The solvent was then removed under reduced pressure. Acetone (∼20 mL) was added to give a suspension, which turned to a clear solution by addition of a small amount of water (∼1 mL). After a short time, the product slowly precipitated and was collected by vacuum filtration. The yield was ∼44% of pale crystals (mp >250 °C, dec). The NIP-*p*NP are poorly soluble in $CHCl_3$, acetone, EtOH, and water but appreciably soluble in DMSO.

1-(1H-Imidazol-2-yl)naphthalen-2-yl p-nitrophenyl phosphate (1NI2P-pNP, Figure S1): ^{1}H NMR (200 MHz, $(CD_3)_2SO$) δ (ppm) 7.30 (2H, d, J = 9.0 Hz), 7.45 (1H, br d, J = 8.8 Hz), 7.50−7.67 (2H, m), 7.73 (1H, d, J = 9.1 Hz), 7.86 (2H, s), 8.05 (1H, br d, J = 8.4 Hz), 8.10−8.26 (3H, m), 14.93 (2H, br s); ^{31}P NMR (81 MHz, $(CD_3)_2SO$) δ (ppm) −11.2; ^{13}C NMR (50 MHz, $(CD_3)_2SO$, coupled to ^{31}P) δ (ppm) 110.7 (d, J = 6.0 Hz), 120.4 (2C, d, J = 5.4 Hz), 120.7 (2C), 122.1, 123.9, 125.7 (2C), 126.0, 128.8, 128.9, 129.9, 132.2, 133.7, 139.5, 142.6, 151.2 (d, J = 6.7 Hz), 159.1 (d, J = 6.5 Hz); ESI-MS, negative-ion mode calcd m/z for $C_{19}H_{13}N_3O_6P^-$ 410.0547, found 410.0548 (100) [M].

2-(1H-Imidazol-2-yl)naphthalen-1-yl p-nitrophenyl phosphate (2NI1P-pNP, Figure S2): ^{1}H NMR (200 MHz, $(CD_3)_2SO$) δ (ppm) 7.40 (2H, d, J = 9.0 Hz), 7.53−7.74 (2H, m), 7.79 (1H, d, J = 8.8 Hz), 7.83 (2H, s), 7.95 (1H, d, J = 8.8 Hz), 8.01 (1H, d, J = 7.6 Hz), 8.20 (2H, d, J = 9.1 Hz), 8.39 (1H, d, J = 8.0 Hz), 15.46 (2H, br s); ^{31}P NMR (81 MHz, $(CD_3)_2SO$) δ (ppm) −9.2; ^{13}C NMR (50 MHz, $(CD_3)_2SO$, coupled to ^{31}P) δ (ppm) 112.7 (d, J = 4.0 Hz), 120.7, 121.1 (2C, d, J = 5.0 Hz), 125.2 (2C, br s), 125.3 (2C, br s), 125.8 (2C), 127.1, 127.9, 128.3 (d, J = 2.0 Hz), 129.0, 136.0, 141.5, 143.2, 147.3 (d, J = 8.1 Hz), 158.6 (d, J = 6.8 Hz). ESI-MS, negative-ion mode calcd m/z for $C_{19}H_{13}N_3O_6P^-$ 410.0547, found 410.0551 (100) [M].

3-(1H-Imidazol-2-yl)naphthalen-2-yl p-Nitrophenyl Phosphate (3NI2P-pNP, Figure S3): ^{1}H NMR (200 MHz, $(CD_3)_2SO$) δ (ppm) 7.47 (2H, d, J = 9.0 Hz), 7.51−7.71 (2H, m), 7.83 (2H, s), 7.89 (1H, s), 7.93−8.06 (2H, m), 8.20 (2H, d, J = 9.1 Hz), 8.38 (1H, s), 15.24 (2H, br s); ^{31}P NMR (81 MHz, $(CD_3)_2SO$) δ (ppm) −9.3; ^{13}C NMR (50 MHz, $(CD_3)_2SO$, coupled to ^{31}P) δ (ppm) 117.3 (d, J = 3.3 Hz), 120.8 (5C, br s), 125.8 (2C), 126.8, 127.7, 128.7, 129.1, 129.5, 131.7, 135.1, 141.4, 143.0, 146.2 (d, J = 7.1 Hz), 158.8 (d, J = 6.5 Hz); ESI-MS, negative-ion mode calcd m/z for $C_{19}H_{13}N_3O_6P^-$ 410.0547, found 410.0549 (100) [M].

Identification of Reaction Species by ^{1}H and ^{31}P NMR. The ^{1}H and ^{31}P NMR spectra (200 MHz for ^{1}H) at different time intervals of the NIP-*p*NP cleavages (4 mg/750 μL) were carried out in NaOD 0.01 M in D_2O at 21 °C. The ^{1}H and ^{31}P chemical shifts were referred to sodium 3-(trimethylsilyl)propionate (TSP, internal reference) and H_3PO_4 85% (external reference), respectively. The relaxation delay was 1s for all acquisitions.

Identification of Reaction Species by ESI-MS(/MS). All experiments were carried out at 19 °C with a hybrid mass spectrometer equipped with ion-trap and time-of-flight technologies (LCMS IT-TOF). The NIP-*p*NP (0.1 mg/10 mL) cleavages were carried out in NaOH 5 mM (1NI2P-*p*NP) or in NH_4OH 5.0 mM (pH 8.5, 2NI1P-*p*NP and 3NI2P-*p*NP). Aliquots of 10 μL of reaction mixture were taken at different time intervals and injected directly into the electrospray ionization (ESI) source. The mass spectrometer operated in negative-ion mode. The species were subjected to collision-induced dissociation (CID) with nitrogen using collision energies of 45 eV.

Kinetic Experiments. Reactions with $t_{1/2}$ < 10 s were followed by spectrophotometry in quartz cuvettes with the temperature controlled with a thermostated water-jacketed cell holder. The ionic strength was kept constant at 1.0 M with KCl. The pH between 3 and 12 was maintained with 0.01 M of the following buffers: HCOOH (pH 3−4.5), CH_3COOH (pH 4−5.5), KH_2PO_4 (pH 5.5−7), Tris-HCl (pH 7−9), $KHCO_3$ (pH 9.2−10.8), and K_2HPO_4 (pH 11.1−12). For kinetic isotope effects using D_2O as solvent, the pD value was determined with a pH meter calibrated with aqueous buffers and corrected considering pD = pH_{read} + 0.4.[61] Absorbance (A) versus time (t) data presented typical first-order kinetic behavior. Data were collected by at least three half-life times ($t_{1/2}$) of reaction, and the observed rate constants (k_{obs}) were calculated using an iterative least-squares program; correlation coefficients were >0.999 for all kinetic runs. The NIP-*p*NP cleavages were monitored by the appearance of products at 342 nm (pH < 6.5) or 405 nm (pH > 6.5). Reactions were started by adding 20 μL of 5 mM stock solution of the substrate in DMSO (stored at −20 °C) into 3 mL of aqueous solutions to give a final concentration of substrate of 33.3 μM.

Reactions in [OH^-] > 0.01 M show $t_{1/2}$ > 10 s and were followed using a stopped-flow spectrophotometer (2 ms dead-time) equipped with synchronous drive system with two syringes of same volume. The reaction solutions were self-buffered with KOH, and no ionic strength correction was made. The content of one syringe consisted of a

DOI: 10.1021/acs.joc.6b01358
J. Org. Chem. 2016, 81, 8663−8672

solution of the substrate (66.6 μM) in water and the other syringe was filled with KOH solution with double the concentration used in the reaction. The reaction was followed over time at 405 nm and exhibited first-order kinetic behaviors. The relationship between H^- and KOH concentration was taken from Bowden.[62]

Nitrogen-15 Kinetic Isotope Effect (^{15}k KIE) Determinations. The ^{15}k KIE was measured using the internal competition method. In the commonly used notation, the ^{15}k KIE denotes isotope effect on the kinetic quantity k_{14}/k_{15}. Natural abundance 1NI2P-*p*NP was used for measurements of ^{15}k. Isotope effect determinations were made at 25 °C in 50 mM Tris buffer, pH 9.0. After reactions reached 40−60% completion, they were stopped by titrating to pH 3−4 with HCl, followed by extraction three times with an equal volume of diethyl ether to remove the *p*-nitrophenol product. The aqueous layer was then made basic, the residual substrate completely hydrolyzed, and the nitrophenol thus liberated was isolated as before. Ether fractions were dried over magnesium sulfate and filtered, ether was removed by rotary evaporation, and the *p*-nitrophenol was purified by sublimation under vacuum at 95 °C. Samples were subjected to nitrogen isotopic analysis using an ANCA-NT combustion system in tandem with an isotope ratio mass spectrometer. Isotope effects were calculated from the nitrogen isotope ratios in the product and residual substrate as previously described.[63]

Computations. Calculations were performed with the Gaussian 09 program[64] at the DFT level using the B3LYP exchange-correlation potential[65,66] and the water dielectric continuum as implemented in the PCM.[67] The 6-31+G(d,p) basis set was used for all atoms. Defaults for convergence and optimization were used without any symmetry constraints. Initial conformations were obtained conventionally. The critical points in the potential energy surface (PES), namely, reactants, products, and transition states, were properly characterized by their force constants, which were all positive, except for the transition state with its imaginary frequency. The transition states were found through a continuous structural search on the PES and then optimized by using an eigenvalue-following algorithm. The charges were obtained with fully optimized structures using the ChelpG procedure.[68]

■ ASSOCIATED CONTENT

Supporting Information

The Supporting Information is available free of charge on the ACS Publications website at DOI: 10.1021/acs.joc.6b01358.

NMR spectra used for characterization of NIP-*p*NP; NMR and ESI-MS spectra at different time intervals of 2NI1P-*p*NP and 3NI2P-*p*NP cleavages; ESI-MS/MS for species in the cleavage of NIP-*p*NP; details about the procedure for EM estimations; thermodynamic data for NIP-*p*NP cleavage; individual energies for structures along the reaction coordinate of NIP-*p*NP cleavage and their Cartesian coordinates (PDF)

■ AUTHOR INFORMATION

Corresponding Author

*Tel: +55 31 3409-5766. Fax: +55 31 3409-5700. E-mail: tasb@ufmg.br.

Notes

The authors declare no competing financial interest.

■ ACKNOWLEDGMENTS

We thank INCT-Catalysis, the Brazilian Foundations MCTI/CNPq (Project Nos. 306498/2013-8 and 484232/2013-4), and FAPEMIG (Project Nos. APQ-01006-13 and APQ-01293-14) for financial support. This work is also part of a collaboration research project of members of the Rede Mineira de Química (RQ-MG) supported by FAPEMIG (Project No. RED-00010-14). We are also grateful to CNPq (Brazil) for a scholarship to M.S.P. and PRONOTURNO/UFMG and PROBIC/FAPEMIG for scholarships to B.M. and T.C.F.O, respectively.

■ REFERENCES

(1) Blain, J. C.; Ricardo, A.; Szostak, J. W. *J. Am. Chem. Soc.* **2014**, *136*, 2033.
(2) Brandsen, B. M.; Velez, T. E.; Sachdeva, A.; Ibrahim, N. A.; Silverman, S. K. *Angew. Chem., Int. Ed.* **2014**, *53*, 9045.
(3) Klumpp, S.; Krieglstein, J. *Sci. Signaling* **2009**, *2*, pe13.
(4) Klumpp, S.; Krieglstein, J. *Eur. J. Biochem.* **2002**, *269*, 1067.
(5) Klumpp, S.; Krieglstein, J. *Biochim. Biophys. Acta, Proteins Proteomics* **2005**, *1754*, 291.
(6) Puttick, J.; Baker, E. N.; Delbaere, L. T. *Biochim. Biophys. Acta, Proteins Proteomics* **2008**, *1784*, 100.
(7) Attwood, P.; Piggott, M.; Zu, X.; Besant, P. *Amino Acids* **2007**, *32*, 145.
(8) Yang, W. *Q. Rev. Biophys.* **2011**, *44*, 1.
(9) Tan, E.; Besant, P. G.; Zu, X. L.; Turck, C. W.; Bogoyevitch, M. A.; Lim, S. G.; Attwood, P. V.; Yeoh, G. C. *Carcinog.* **2004**, *25*, 2083.
(10) Besant, P. G.; Attwood, P. V. *Int. J. Biochem. Cell Biol.* **2000**, *32*, 243.
(11) Matthews, H. R. *Pharmacol. Ther.* **1995**, *67*, 323.
(12) Kim, Y.; Pesis, K. H.; Matthews, H. R. *Biochim. Biophys. Acta, Mol. Cell Res.* **1995**, *1268*, 221.
(13) Selvy, P. E.; Lavieri, R. R.; Lindsley, C. W.; Brown, H. A. *Chem. Rev.* **2011**, *111*, 6064.
(14) Clore, G. M.; Venditti, V. *Trends Biochem. Sci.* **2013**, *38*, 515.
(15) Nishimura, J. S. *Adv. Enzymol. Relat. Areas Mol. Biol.* **2006**, *58*, 141.
(16) Janin, J.; Deville-Bonne, D. *Methods Enzymol.* **2002**, *354*, 118.
(17) Ghosh, A.; Shieh, J.-J.; Pan, C.-J.; Sun, M.-S.; Chou, J. Y. *J. Biol. Chem.* **2002**, *277*, 32837.
(18) Rigden, D. J. *Biochem. J.* **2008**, *409*, 333.
(19) Veeramani, S.; Lee, M. S.; Lin, M. F. *Trends Biochem. Sci.* **2009**, *34*, 273.
(20) Exton, J. H. *Rev. Physiol. Biochem. Pharmacol.* **2002**, *144*, 1.
(21) DeYonker, N. J.; Webster, C. E. *Biochemistry* **2015**, *54*, 4236.
(22) Henage, L. G.; Exton, J. H.; Brown, H. A. *J. Biol. Chem.* **2006**, *281*, 3408.
(23) Schroeder, G. K.; Lad, C.; Wyman, P.; Williams, N. H.; Wolfenden, R. *Proc. Natl. Acad. Sci. U. S. A.* **2006**, *103*, 4052.
(24) Kirby, A. J.; Hollfelder, F. *Nature* **2008**, *456*, 45.
(25) DeYonker, N. J.; Webster, C. E. *J. Am. Chem. Soc.* **2013**, *135*, 13764.
(26) Orth, E. S.; Brandao, T. A. S.; Souza, B. S.; Pliego, J. R.; Vaz, B. G.; Eberlin, M. N.; Kirby, A. J.; Nome, F. *J. Am. Chem. Soc.* **2010**, *132*, 8513.
(27) NIP-*p*NP is used to refer to the series of compounds, while 1NI2P-*p*NP, 2NI1P-*p*NP, and 3NI2P-*p*NP refer to particular compounds. To distinguish ionic species, we use a superscript charge, e.g., 1NI2P-*p*NP^- for the monoanionic species of 1NI2P-*p*NP. We also use the abbreviation NIP*c* for the cyclic aryl phosphoimidazoles formed from each NIP-*p*NP cleavage.
(28) Catalán, J.; del Valle, J. C.; Palomar, J.; Díaz, C.; de Paz, J. L. *J. Phys. Chem. A* **1999**, *103*, 10921.
(29) Oliveira, T. C.; Carmo, L. F.; Murta, B.; Duarte, L. G.; Nome, R. A.; Rocha, W. R.; Brandao, T. A. S. *Phys. Chem. Chem. Phys.* **2015**, *17*, 2404.
(30) Catalan, J.; del Valle, J. C. *J. Am. Chem. Soc.* **1993**, *115*, 4321.
(31) Kezdy, F. J.; Bender, M. L. *Biochemistry* **1962**, *1*, 1097.
(32) Martell, A. E.; Smith, Z. M.; Motekaitis, R. J. *NIST Critical Stability Constants of Metal Complexes Database Version 8 (for Windows): NIST Standard Reference Database 46*; NIST: Gaithersburg, 2004.
(33) Gadsby, P. M. A.; Thomson, A. J. *FEBS Lett.* **1982**, *150*, 59.
(34) George, P.; Hanania, G. I. H.; Irvine, D. H.; Abuissa, I. *J. Chem. Soc.* **1964**, 5689.
(35) Rogers, G. A.; Bruice, T. C. *J. Am. Chem. Soc.* **1974**, *96*, 2463.

DOI: 10.1021/acs.joc.6b01358
J. Org. Chem. 2016, 81, 8663−8672

(36) Chin, J.; Banaszczyk, M.; Jubian, V.; Zou, X. *J. Am. Chem. Soc.* **1989**, *111*, 186.
(37) Kirby, A. J.; Souza, B. S.; Nome, F. *Can. J. Chem.* **2015**, *93*, 422.
(38) Kirby, A. J.; Nome, F. *Acc. Chem. Res.* **2015**, *48*, 1806.
(39) Orth, E. S.; Wanderlind, E. H.; Medeiros, M.; Oliveira, P. S. M.; Vaz, B. G.; Eberlin, M. N.; Kirby, A. J.; Nome, F. *J. Org. Chem.* **2011**, *76*, 8003.
(40) Kirby, A. J.; Younas, M. *J. Chem. Soc. B* **1970**, 1165.
(41) Lazarus, R. A.; Benkovic, P. A.; Benkovic, S. J. *J. Chem. Soc., Perkin Trans. 2* **1980**, 373.
(42) Loran, J. S.; Williams, A. *J. Chem. Soc., Perkin Trans. 2* **1977**, 64.
(43) Kirby, A. J.; Medeiros, M.; Mora, J. R.; Oliveira, P. S. M.; Amer, A.; Williams, N. H.; Nome, F. *J. Org. Chem.* **2013**, *78*, 1343.
(44) Bruice, T. C.; Brown, A.; Harris, D. O. *Proc. Natl. Acad. Sci. U. S. A.* **1971**, *68*, 658.
(45) Bruice, T. C. *Nature* **1972**, *237*, 335.
(46) Menger, F. M. *Tetrahedron* **1983**, *39*, 1013.
(47) Domingos, J. B.; Longhinotti, E.; Brandão, T. A. S.; Santos, L. S.; Eberlin, M. N.; Bunton, C. A.; Nome, F. *J. Org. Chem.* **2004**, *69*, 7898.
(48) Dixon, J. E.; Stuckey, J. A. *Nat. Struct. Biol.* **1999**, *6*, 278.
(49) Kirby, A. J.; Hollfelder, F. *From Enzyme Models to Model Enzymes*; RSC: London, 2009.
(50) Ekici, O. D.; Paetzel, M.; Dalbey, R. E. *Protein Sci.* **2008**, *17*, 2023.
(51) Hedstrom, L. *Chem. Rev.* **2002**, *102*, 4501.
(52) Frey, P. A. *J. Biol. Chem.* **2015**, *290*, 10610.
(53) Komiyama, M. *Bull. Chem. Soc. Jpn.* **1990**, *63*, 626.
(54) Kirby, A. J.; Manfredi, A. M.; Souza, B. S.; Medeiros, M.; Priebe, J. P.; Brandão, T. A. S.; Nome, F. *ARKIVOC* **2009**, *3*, 28.
(55) Hengge, A. C. *FEBS Lett.* **2001**, *501*, 99.
(56) Catrina, I. E.; Hengge, A. C. *J. Am. Chem. Soc.* **2003**, *125*, 7546.
(57) Bruice, T. C.; Lightstone, F. C. *Acc. Chem. Res.* **1999**, *32*, 127.
(58) Bruice, T. C. *Acc. Chem. Res.* **2002**, *35*, 139.
(59) Bruice, T. C. *Chem. Rev.* **2006**, *106*, 3119.
(60) Li, L.; Lelyveld, V. S.; Prywes, N.; Szostak, J. W. *J. Am. Chem. Soc.* **2016**, *138*, 3986.
(61) Schowen, K. B. J. In *Transition States of Biochemical Processes*; Gandour, R. D., Ed.; Plenum: New York, 1978; p 225.
(62) Bowden, K. *Chem. Rev.* **1966**, *66*, 119.
(63) Hengge, A. C. *Acc. Chem. Res.* **2002**, *35*, 105.
(64) Frisch, M. J.; Trucks, G. W.; Schlegel, H. B.; Scuseria, G. E.; Robb, M. A.; Cheeseman, J. R.; Scalmani, G.; Barone, V.; Mennucci, B.; Petersson, G. A.; Nakatsuji, H.; Caricato, M.; Li, X.; Hratchian, H. P.; Izmaylov, A. F.; Bloino, J.; Zheng, G.; Sonnenberg, J. L.; Hada, M.; Ehara, M.; Toyota, K.; Fukuda, R.; Hasegawa, J.; Ishida, M.; Nakajima, T.; Honda, Y.; Kitao, O.; Nakai, H.; Vreven, T.; Montgomery, J. A., Jr.; Peralta, J. E.; Ogliaro, F.; Bearpark, M. J.; Heyd, J.; Brothers, E. N.; Kudin, K. N.; Staroverov, V. N.; Kobayashi, R.; Normand, J.; Raghavachari, K.; Rendell, A. P.; Burant, J. C.; Iyengar, S. S.; Tomasi, J.; Cossi, M.; Rega, N.; Millam, N. J.; Klene, M.; Knox, J. E.; Cross, J. B.; Bakken, V.; Adamo, C.; Jaramillo, J.; Gomperts, R.; Stratmann, R. E.; Yazyev, O.; Austin, A. J.; Cammi, R.; Pomelli, C.; Ochterski, J. W.; Martin, R. L.; Morokuma, K.; Zakrzewski, V. G.; Voth, G. A.; Salvador, P.; Dannenberg, J. J.; Dapprich, S.; Daniels, A. D.; Farkas, Ö.; Foresman, J. B.; Ortiz, J. V.; Cioslowski, J.; Fox, D. J. *Gaussian 09*; Gaussian, Inc.: Wallingford, CT, 2009.
(65) Becke, A. D. *J. Chem. Phys.* **1993**, *98*, 5648.
(66) Lee, C.; Yang, W.; Parr, R. G. *Phys. Rev. B: Condens. Matter Mater. Phys.* **1988**, *37*, 785.
(67) Tomasi, J.; Mennucci, B.; Cammi, R. *Chem. Rev.* **2005**, *105*, 2999.
(68) Breneman, C. M.; Wiberg, K. B. *J. Comput. Chem.* **1990**, *11*, 361.

DOI: 10.1021/acs.joc.6b01358
J. Org. Chem. 2016, 81, 8663−8672